Carrier-carrier scattering and optical dephasing in highly excited semiconductors

R. Binder, D. Scott, A. E. Paul, M. Lindberg, K. Henneberger,* and S. W. Koch
Optical Sciences Center and Physics Department, University of Arizona, Tucson, Arizona 85721
(Received 3 June 1991; revised manuscript received 3 September 1991)

A quantitative analysis of carrier-carrier scattering and optical dephasing in semiconductors is presented and results are given for quasiequilibrium situations and for the relaxation of a kinetic hole in a quasithermal carrier distribution. The calculations involve direct numerical integration of the Boltzmann equation for carrier-carrier scattering in the Born approximation. The screening of the Coulomb interaction is treated consistently in the fully dynamical random-phase approximation. Carrier relaxation rates are extracted from the Boltzmann-equation solution and a quantitative test of the relaxation-time approximation for situations near thermal quasiequilibrium is performed. The parametric dependence of carrier-collision rates and dephasing on plasma density, temperature, and electron and hole masses is discussed and analyzed in terms of phase-space blocking and screening.

I. INTRODUCTION

Carrier-carrier (*cc*) scattering in highly excited semiconductors is often the dominant relaxation mechanism which drives the system toward a quasiequilibrium state. Of particular interest are situations where (i) an initial nonequilibrium carrier distribution evolves into a quasiequilibrium state and (ii) a nonequilibrium condition exists in a steady state.

A generic example for the first situation is an optically pumped semiconductor, where electron-hole pairs are generated by short-pulse interband excitation.[1–4] This kind of experiment in intrinsic, *p*- or *n*-type doped semiconductors makes it possible to investigate scattering in a neutral electron-hole plasma, or in a hole or electron plasma, respectively.[2] Optical femtosecond pump and probe techniques allow time-resolved observation of the relaxation processes by monitoring the spectral changes caused by the temporal evolution of the carrier distribution function, which may lead to a spectral hole in the continuum absorption or in the optical gain.[4,5]

The situation of a quasistationary nonequilibrium carrier distribution is realized, e.g., in a cw running semiconductor laser, where electron-hole pairs are constantly generated through injection pumping and removed mostly through stimulated emission. The frequency-selective carrier removal tends to cause a kinetic hole in the quasiequilibrium carrier distribution which would be present without the running laser mode. The detailed shape of the kinetic hole is determined by the interplay between stimulated recombination and carrier-carrier scattering.

Generally, other mechanisms besides carrier-carrier scattering exist that contribute to the total relaxation. Examples are LO-phonon and acoustic-phonon scattering, i.e., deformation-potential and piezoelectric scattering.[6,7] However, carrier-carrier collisions provide the dominant relaxation channel for situations with very high carrier densities,[2,8] or low temperatures and carrier excitation below the LO-phonon threshold.[9]

The theoretical basis of *cc* scattering and its consequences, like energy-level broadening and screening of the Coulomb potential, can be found in the many-body-theory literature, e.g., Refs. 10 and 11, and we therefore restrict our presentation to a brief summary of the essential equations in Sec. II of this paper. For our purposes it is especially important to emphasize the relation of the carrier scattering rates with the optical dephasing, i.e., the temporal decay of the interband polarization. The *cc* dephasing turns out to be the average of the total electron (*e*) and hole (*h*) relaxation rates.

Although many publications deal with *cc* scattering rates and time evolutions for distribution functions,[12–21] electron-energy-loss rates,[18] and electron-hole energy transfer rates,[17] it is still difficult to perform a direct numerical integration of the Boltzmann equation where the screening is treated on the same footing as the scattering probabilities. We present in this paper a solution for the scattering rates within the Born approximation including the screening of the Coulomb potential in the full dynamical random-phase approximation (RPA). In Sec. III we evaluate the Boltzmann equation for the relaxation of a kinetic hole in a high-density quasiequilibrium carrier distribution. This situation is most relevant in semiconductor lasers and amplifiers. From the full solution of the Boltzmann equation we extract carrier relaxation rates and investigate the applicability of the so-called relaxation-time approximation (RTA).

In Sec. III we also present a detailed discussion of the dependence of the carrier relaxation rates on relevant material parameters such as the electron and hole masses, the plasma density, and the optical pump frequency. The effective masses of holes and electrons in semiconductors and semiconductor quantum wells differ by factors of the order of 1 to 10. Therefore, the phase-space effects (Pauli blocking) are quantitatively quite different for electrons and holes. For doped semiconductors this leads to different scattering rates in *n*- or *p*-type materials.[2] For a two-component electron-hole (*e*-*h*) plasma, the scattering rates depend on the *e*-*h* mass ratio. A short summary

in Sec. IV concludes the paper. In the appendixes we present some details of our numerical methods (Appendix A) and of the relaxation rate approximation (Appendix B). Furthermore, in Appendix B we also give some useful analytical fitting formulas for the chemical potential and the effective carrier temperature for quasiequilibrium Fermi distributions.

II. OPTICAL DEPHASING AND THE BOLTZMANN EQUATION FOR CARRIER-CARRIER SCATTERING

Optical nonlinearities in highly excited semiconductors can be modeled using a generalization of the semiclassical optical Bloch equations for the polarization $P(k,t)$ of the momentum state k and the distribution functions of electrons and holes $f_\alpha(k,t)$, $\alpha=e,h$.[22-26] For the purposes of this paper we restrict the discussion to the limit of high plasma densities, allowing us to neglect the *eh* Coulomb correlation. In this limit the semiconductor Bloch equations are

$$\left[i\hbar\frac{\partial}{\partial t}-\varepsilon_e(k)-\Sigma_r^e(k)-\varepsilon_h(k)-\Sigma_r^h(k)+i\gamma_0\right]P(k) =\mu^{cv}E[1-f_e(k)-f_h(k)] \quad (2.1)$$

and

$$\hbar\frac{df_\alpha(k_1)}{dt}=2\,\mathrm{Im}[(\mu^{cv}E)^*P(k)]+\hbar\left.\frac{df_\alpha(k_1)}{dt}\right|_{cc}, \quad (2.2)$$

where the carrier-carrier scattering term is given by the Boltzmann equation

$$\left.\frac{df_\alpha(k_1)}{dt}\right|_{cc}=\Gamma_{\mathrm{in}}^\alpha[k_1,f][1-f_\alpha(k_1)] -\Gamma_{\mathrm{out}}^\alpha[k_1,f]f_\alpha(k_1)\ . \quad (2.3)$$

Equations (2.1) and (2.2) describe the response of a two-band semiconductor with optical dipole matrix element μ^{cv} to a classical external field E. In Eq. (2.1) the renormalization of the unperturbed energy bands

$$\varepsilon_\alpha(k)=\hbar^2k^2/2m_\alpha+\varepsilon_\alpha(0) \quad (2.4)$$

($m_e,m_h>0$) due to *cc* scattering is described by the retarded self-energy $\Sigma_r^\alpha(k,\omega)$. For simplicity, we treat the frequency dependence of the self-energy in a quasiparticle approximation based on the fact that the quasiparticle dispersion for electrons or holes follows from

$$E_\alpha(k)=\varepsilon_\alpha(k)+\mathrm{Re}\Sigma_r^\alpha[k,E_\alpha(k)] \simeq\varepsilon_\alpha(k)+\mathrm{Re}\Sigma_r^\alpha(k)\ ,$$

where $\Sigma_r^\alpha(k)\equiv\Sigma_r^\alpha[k,\varepsilon_\alpha(k)]$.[11] Renormalization and broadening of the state k are therefore approximately given by the real and imaginary parts of $\Sigma_r^\alpha(k)$, respectively.

The dephasing rate γ_0 in Eq. (2.1) comprises all processes that contribute to the decay of the optical polarization in the limit of vanishing plasma density. The additional dephasing due to the carrier plasma can be described by the dephasing time T_2' defined as

$$\frac{\hbar}{T_2'}=-\,\mathrm{Im}[\Sigma_r^e(k)+\Sigma_r^h(k)]\ . \quad (2.5)$$

This time is governed by the fast *cc* intraband scattering, not by the *eh* interband recombination as could be expected in analogy to atomic systems. The relaxation of the distribution function toward a thermal quasiequilibrium is described by the in and out scattering rates Γ_{in} and Γ_{out}. The dephasing rate of one-particle states is quite generally related to the retarded self-energy via[6,11,15]

$$\hbar(\Gamma_{\mathrm{in}}^\alpha+\Gamma_{\mathrm{out}}^\alpha)=-2\,\mathrm{Im}\Sigma_r^\alpha\ . \quad (2.6)$$

As we discuss in Sec. III in more detail, it is possible to define the total scattering rate Γ for plasmas close to quasithermal equilibrium via

$$\Gamma^\alpha=\Gamma_{\mathrm{in}}^\alpha+\Gamma_{\mathrm{out}}^\alpha\ . \quad (2.7)$$

Introducing the longitudinal intraband relaxation time T_1' by $\Gamma=1/T_1'$ we have the usual relationship $T_2=2T_1'$, here specialized for the case of *cc* scattering. A discussion of more sophisticated dephasing theories (i.e., beyond the quasiparticle approximation) can be found, e.g., in Ref. 6.

In order to describe a laser, one has to treat the light field self-consistently with the material polarization. The relationship of the decay of the photon correlation function with the dephasing processes presented here can be found, e.g., in Refs. 27 and 28. Additionally, in the laser case the equations for f must be supplemented by contributions describing injection pumping and spontaneous emission.

The carrier-carrier scattering rates within the Born approximation are derived and qualitatively discussed in many publications (see, e.g., Ref. 11). Therefore, we just summarize the basic results:[29]

$$\Gamma_{\mathrm{in}}^e[\mathbf{k}_1,f]=\frac{2\pi}{\hbar}\sum_{\alpha,\mathbf{k}_2,\mathbf{k}_3,\mathbf{k}_4}2|W[\mathbf{k}_2-\mathbf{k}_1,\varepsilon_e(k_2)-\varepsilon_e(k_1)]|^2f_e(k_2)[1-f_\alpha(k_3)]f_\alpha(k_4) \times\delta_{\mathbf{k}_1+\mathbf{k}_3,\mathbf{k}_2+\mathbf{k}_4}\delta[\varepsilon_e(k_1)-\varepsilon_e(k_2)+\varepsilon_\alpha(k_3)-\varepsilon_\alpha(k_4)] \quad (2.8)$$

and

$$\Gamma_{\mathrm{out}}^e[\mathbf{k}_1,f]=\frac{2\pi}{\hbar}\sum_{\alpha,\mathbf{k}_2,\mathbf{k}_3,\mathbf{k}_4}2|W[\mathbf{k}_2-\mathbf{k}_1,\varepsilon_e(k_2)-\varepsilon_e(k_1)]|^2[1-f_e(k_2)]f_\alpha(k_3)[1-f_\alpha(k_4)] \times\delta_{\mathbf{k}_1+\mathbf{k}_3,\mathbf{k}_2+\mathbf{k}_4}\delta[\varepsilon_e(k_1)-\varepsilon_e(k_2)+\varepsilon_\alpha(k_3)-\varepsilon_\alpha(k_4)]\ , \quad (2.9)$$

where W denotes the screened Coulomb potential. The corresponding hole scattering rates are obtained from Eqs. (2.8) and (2.9) by substituting h for the index e. We always assume the distribution functions to be isotropic, i.e., to depend only $|\mathbf{k}|$.

The screened Coulomb potential is given as

$$W(q,\omega)=\frac{V(q)}{1-V(q)P(q,\omega)}=V(q)\epsilon^{-1}(q,\omega)\ , \tag{2.10}$$

containing the unscreened potential

$$V(q)=\frac{4\pi e^2}{Vq^2}\ , \tag{2.11}$$

which includes the background dielectric constant of the unexcited material ϵ_0 via $e^2=e_0^2/\epsilon_0$ (e_0 is the free electron charge) and V is the crystal volume. Within the Born approximation for the scattering rates the dynamical screening due to the charge carriers is determined by the RPA intraband polarization function[30]

$$P(\mathbf{q},\omega)=\lim_{\delta\to 0}2\sum_{\alpha,\mathbf{k}}\frac{f_\alpha(k)-f_\alpha(|\mathbf{q}+\mathbf{k}|)}{\varepsilon_\alpha(k)-\varepsilon_\alpha(|\mathbf{q}+\mathbf{k}|)+\hbar\omega+i\delta}\ . \tag{2.12}$$

We want to point out that within the Born approximation the quasiequilibrium scattering rates take the familiar form ($\propto \mathrm{Im}W$) only if one uses the full RPA screening function.

The effects of phase-space filling due to Fermi statistics and the screening of the Coulomb potential generally prevent the scattering rates from increasing monotonically with the density of the plasma. These effects are not mutually independent since, as shown by Eq. (2.12), the screening itself is affected by phase-space filling. In the classical limit, when the distribution functions are small in comparison to unity, the density dependence of the scattering rates is dominated by screening. Therefore, at low densities an increase of the carrier density makes more particles available for scattering but the matrix element for each scattering event is reduced. At higher densities the situation is more complicated due to phase-space filling which depends strongly on the masses of the two plasma components.

III. RESULTS AND DISCUSSION

We solve the Boltzmann equation (2.3) together with Eqs. (2.8)–(2.12) numerically using the techniques described in Appendix A. As a relevant material for our studies we choose bulk GaAs, where $\epsilon_0=12.3$ and the exciton binding energy is $E_r=4.2$ meV, which corresponds to a Bohr radius of $a_B=140$ Å within a two-band model. Since we are using the two-band model we approximate the heavy- and light-hole bands, which are degenerate at $k=0$, by one effective band. The choice of the averaged hole mass is not unambiguous. Therefore, we investigate the influence of the average hole mass or, more precisely, the influence of the mass ratio m_h/m_e for a fixed reduced mass $(1/m_e+1/m_h)^{-1}$. As model parameters we choose $m_e=0.067m_0$ and $m_h=0.247m_0$ (m_0 being the free-electron mass), corresponding to a mass ratio $m_h/m_e=3.68$. This value for m_h is obtained simply by averaging the heavy-hole mass $m_{\mathrm{hh}}=0.37m_0$ and the light hole mass $m_{\mathrm{lh}}=0.08m_0$ so that the density of states of the averaged hole band yields the average of the density of states of the two hole bands, i.e., $m_h^{3/2}=\frac{1}{2}(m_{\mathrm{hh}}^{3/2}+m_{\mathrm{lh}}^{3/2})$.

We study the situation where the distribution function has been distorted at small k values, as would happen due to an optical pump beam with a central frequency in the gain region of an inverted semiconductor. Figures 1(a) and 1(b) show the relaxation of such a "kinetic hole" in the electron and hole distribution functions. The kinetic hole in both distributions vanishes very rapidly, on the time scale of 50–100 fs. The corresponding dephasing time $T_2'=2/(\Gamma^e+\Gamma^h)\simeq 50$ fs.

To study the validity of the relaxation-time approximation (RTA) discussed in Appendix B, Eq. (B2), we extract

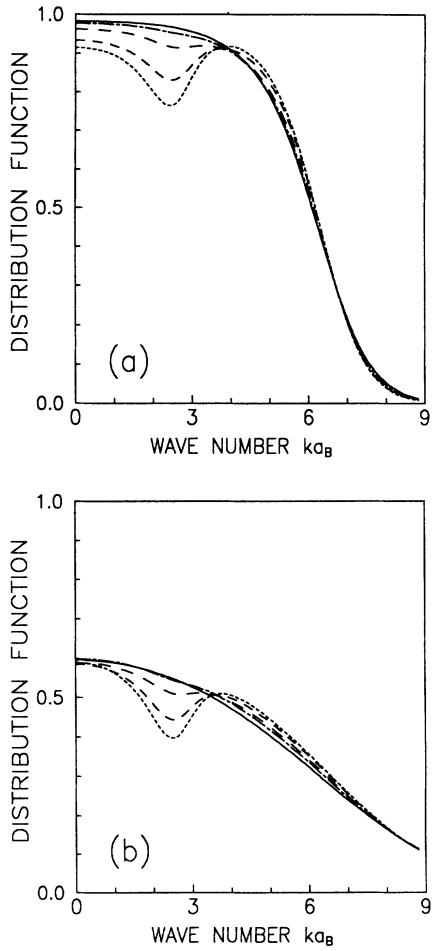

FIG. 1. Relaxation of initially disturbed Fermi distribution functions for density $n=3\times10^{18}$ cm^{-3} and temperature $T\simeq 300$ K obtained by numerically solving the Boltzmann equation using the dynamically screened Coulomb potential in the RPA. Shown are the distribution functions of electrons (a) and holes (b) as functions of the carrier momentum in units of a_B^{-1}. The initial ($t=0$) distribution functions are shown as dotted lines. Consecutive times are $t=21$ fs (short-dashed line), $t=75$ fs (long-dashed line), and $t=147$ fs (dash-dotted line), and the final time $t=796$ fs (solid line).

diagonal relaxation rates using the numerical results of Fig. 1. These relaxation rates are plotted in Figs. 2(a) and 2(b), for electrons and holes, respectively. The relaxation rates at the center of the spectral hole are $\Gamma_e \simeq 22.1\ \mathrm{ps}^{-1}$ and $\Gamma_h \simeq 18.2\ \mathrm{ps}^{-1}$, corresponding to relaxation times of 45.2 fs for the electrons and 54.9 fs for the holes, respectively. Using these relaxation rates, we solve Eq. (B2) for the same initial condition as Fig. 1. The qualitative results are almost indistinguishable from those in Fig. 1. Therefore, in order to investigate the subtle differences between the relaxation rate approximation and the full Boltzmann equation solution, we plot in Fig. 3 the difference, $\Delta f_i(t) \equiv f_i(t) - f_i(t_\infty)$, between the actual distribution functions at time t and the final distribution function using the respective curves in Fig. 1 and those obtained in the RTA. We choose t_∞ as the longest time in these plots, i.e., $t_\infty \simeq 0.8$ ps. Figure 3 shows that even though the RTA results are remarkably close to the full results, they do not reproduce the dynamic reshaping of the kinetic holes, especially at later times in the relaxation process. This reshaping is a consequence of nondiagonal relaxation, i.e., scattering of carriers between different k states. For a qualitative analysis of the relaxation of slightly disturbed quasiequilibrium distributions, optical dephasing, and related phenomena, where fine details of the kinetic hole play no significant role, the RTA can safely be used, provided that the relaxation rates are computed properly.

In the remainder of this section we study various parametric dependencies of the relaxation rates for the quasiequilibrium. To investigate the mass ratio dependence we choose a high plasma density (here $n = 3 \times 10^{18}$ cm^{-3}) and room temperature $T = 300$ K. Figure 4 shows the relaxation rates of electrons and holes for various mass ratios m_h/m_e, all other parameters remain unchanged. As usual, the electron relaxation rates show a minimum where the distribution switches from occupied to unoccupied due to phase-space restrictions.[12] For the mass ratio $m_h/m_e = 3.68$ one has much less phase-space restriction for the holes than for the electrons leading to an almost k-independent hole scattering rate. For electrons and holes the scattering rates are both $\simeq 20\ \mathrm{ps}^{-1}$, so that an initial disturbance of the Fermi distribution function at a given k value would experience an exponential decay with the time constant $\simeq 50$ fs. This result is not much different for a semiconductor with equal electron and hole masses ($m_h/m_e = 1$), except for the fact that now the hole also exhibits reduced relaxation near the Fermi wave number k_F. More pronounced changes

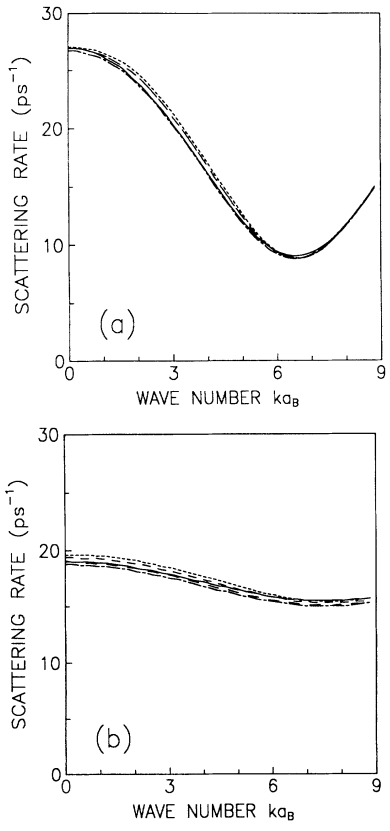

FIG. 2. Carrier-carrier scattering rates extracted from Fig. 1. (a) Electrons; (b) holes.

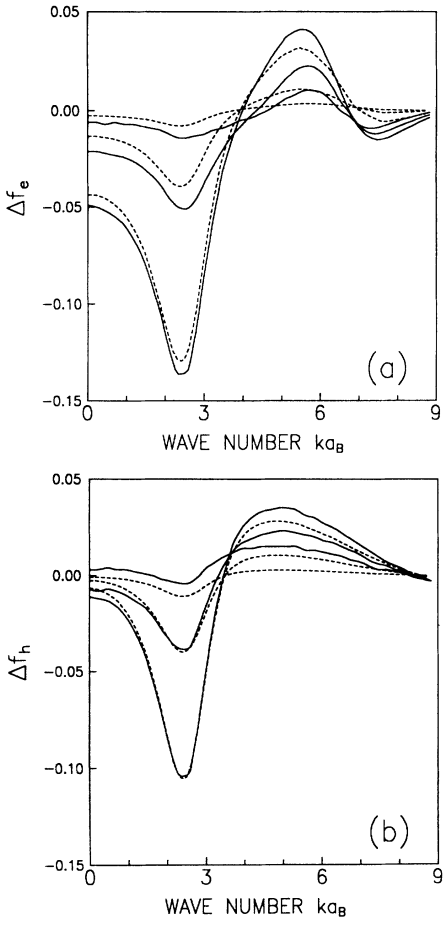

FIG. 3. Difference of carrier distribution functions $\Delta f_e = f_e(t) - f_e(t_\infty)$ and Δf_h obtained from the results in Fig. 1 (solid lines) and the corresponding relaxation rate approximation (dashed lines), Eq. (B2), using the relaxation rates of Fig. 2 at the maximum of the kinetic hole. For t_∞ we took 0.8 ps and the other times are 21, 75, and 147 fs, respectively. The small substructures in the RPA result indicate our numerical accuracy.

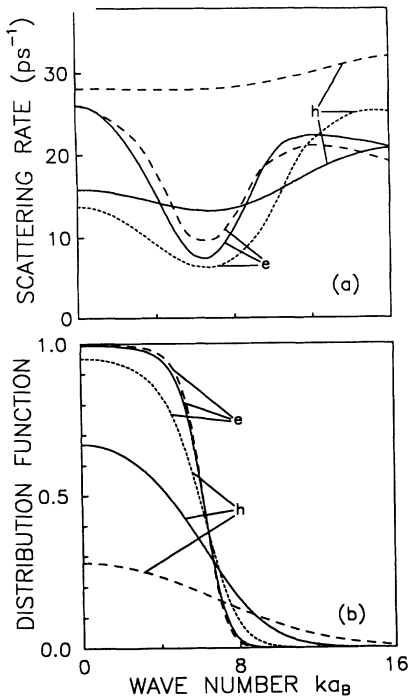

FIG. 4. (a) Carrier-carrier scattering rates of electrons and holes in the presence of an electron-hole plasma in bulk GaAs in quasithermal equilibrium at a temperature of $T=300$ K and a density of $n=3\times10^{18}$ cm^{-3}. The electron-hole mass ratio is $m_h/m_e=3.68$ (solid line), $m_h/m_e=1.0$ (short-dashed line), and $m_h/m_e=10$ (long-dashed line). (b) The corresponding Fermi distribution functions.

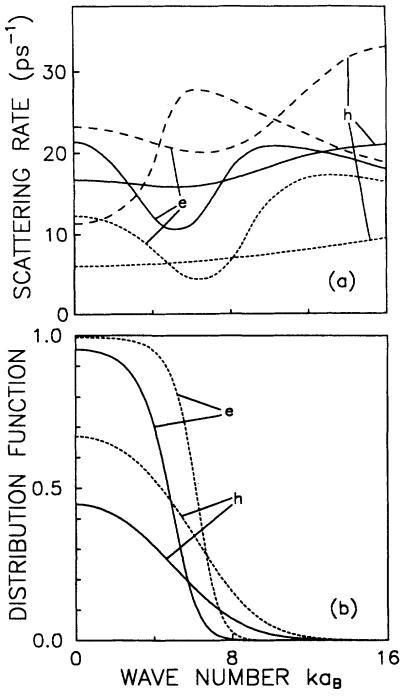

FIG. 5. (a) Equilibrium scattering rates for $m_h/m_e=3.68$. The different curves are for a double-component (electron-hole) plasma with electron-hole density $n=1.5\times10^{18}$ cm^{-3} (solid line), for a single-component plasma of electrons at a density of $n=3\times10^{18}$ cm^{-3} (short-dashed line), and for a single-component plasma of holes of a density of $n=3\times10^{18}$ cm^{-3} (long-dashed line). (b) The corresponding Fermi distribution functions for the electron-hole plasma are the solid curves, and those of the single-component electron and hole plasmas are the short-dashed curves.

occur for systems with very unequal masses. Figure 4 shows the case of $m_h/m_e=10$, where the holes experience hardly any phase-space restrictions. This situation is accompanied by a strong enhancement of the relaxation rate of the holes which now correspond to a time constant of only 35 fs.

To investigate the relative influence of phase-space filling and screening, we compare in Fig. 5 the relaxation rates for a single-component electron plasma and a single component hole plasma, thereby modeling the cases of n- or p-type doped semiconductors. We also show the results for a double-component electron-hole plasma with half the density of the single-component plasma, so that the total particle densities are the same in all cases. However, because of the different masses the plasma frequency $\omega_{\rm pl}$ varies between the curves, in contrast to the examples shown in Fig. 4 which all correspond to the same plasma frequency (same reduced mass). The plasma frequency $\hbar\omega_{\rm pl}/E_r\simeq18$ for the single-component electron plasma in Fig. 6, $\hbar\omega_{\rm pl}/E_r\simeq14$ for the double-component plasma, and $\hbar\omega_{\rm pl}/E_r\simeq9$ for the single-component hole plasma, respectively. It is quite striking that the hole relaxation rates, which are less dominated by pure phase-space restriction than the electron relaxation rates, are roughly inversely proportional to the plasma frequency, showing that screening slows down the carrier equilibration process in a more or less k-independent fashion. The electron relaxation rates in Fig. 5 exhibit strong phase-space effects for the case of a single-component electron plasma, and somewhat reduced phase-space modifications for the half-density double-component plasma. In the case of a single-component hole plasma the electrons can thermalize most effectively except at small k values.

Usually, in doped semiconductors the background carrier density is not quite as high as in optical excitation experiments. Therefore, we calculate the scattering rates for a plasma of density $n=3\times10^{17}$ cm^{-3} at room temperature. The comparison of Figs. 4 and 6 for the double-component plasma with mass ratio $m_h/m_e=3.68$ shows that a reduced density "washes out" the structure in the electron relaxation rate, since the distribution function is not strongly degenerate. Both e and h scattering rates do not change drastically as the density is reduced, indicating again the twofold role of the carriers: (i) fewer carriers lead to fewer scattering events and thus to a decrease of the scattering rates; and (ii) fewer carriers lead to increased scattering cross sections because the screening of the Coulomb potential is reduced.

The comparison of Figs. 5 and 6 for the single component plasmas and for the corresponding half-density eh plasma shows that most of the features found in the high-density case still occur at reduced density. Of course, for lower densities the e-scattering rates exhibit

less structure and all scattering rates are slightly increased in comparison to Fig. 5. We attribute this to the reduction of screening, which overcompensates the effect of a reduced number of scattering partners.

The fact that Figs. 5 and 6 both show larger scattering rates if the single-component plasma consists of heavy particles (h plasma) compared to a light-particle plasma (e plasma) is not in contradiction to Ref. 21, where it has been found that for n-type doped systems at zero temperature and for $k=0$ the scattering rate decreases with increasing mass. In that case, the phase-space restriction is the dominant contribution and our results yield similar behavior for $k=0$ and $T\simeq 0$. For a cold (10 K) eh plasma we show in Fig. 7 the influence of the mass ratio on the scattering rates. At low temperatures and small k values the heavier particles relax at a much reduced rate compared to the lighter particles. However, we cannot confirm the room-temperature results of Ref. 2, where strongly increased scattering rates in the case of n-type doped as opposed to p-type doped quantum wells have been reported.

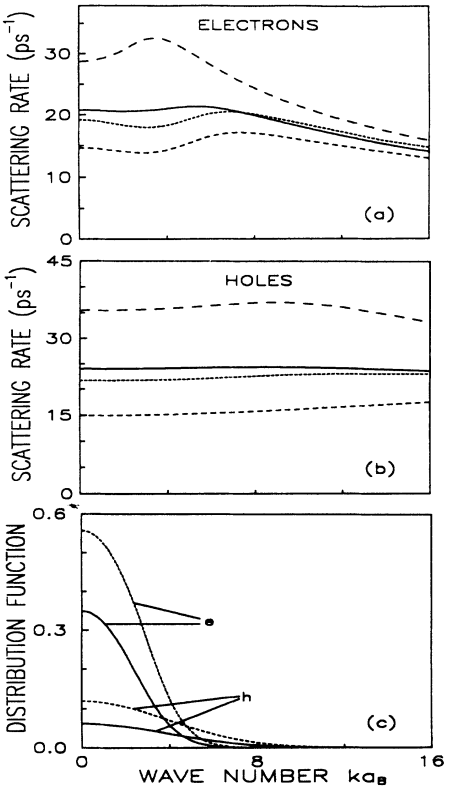

FIG. 6. Equilibrium scattering rates corresponding to Fig. 4. The different curves are for a double-component plasma of electrons (a) and holes (b) each having a density of 1.5×10^{17} cm^{-3} (solid line), 3×10^{17} cm^{-3} (short-dashed line), for a single-component plasma of electrons at a density of $n=3\times10^{17}$ cm^{-3} (medium-dashed line), and for a single-component plasma of holes at a density of $n=3\times10^{17}$ cm^{-3} (long-dashed line). $T=300$ K for all curves. (c) The corresponding Fermi distribution functions for the electron-hole plasma are the solid curves, and those of the single-component electron and hole plasmas are short-dashed curves.

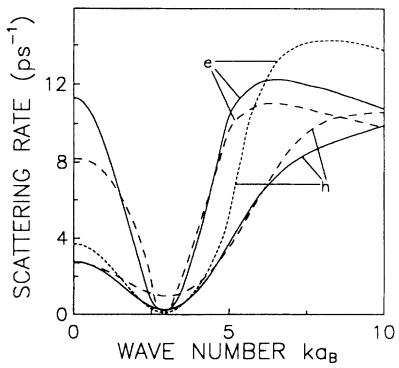

FIG. 7. Equilibrium scattering rates for $T=10$ K and eh plasma density $n=3\times10^{17}$ cm^{-3}. The different curves are for mass ratios of $m_h/m_e=3.68$ (solid line), $m_h/m_e=1.0$ (short-dashed line), and $m_h/m_e=10$ (long-dashed line).

IV. SUMMARY AND CONCLUSIONS

In summary, we present a quantitative analysis of scattering and dephasing rates for electron, hole, and electron-hole plasmas in semiconductors. Scattering rates and dynamical screening are treated on an equal footing. We study carrier relaxation for situations in and near quasithermal equilibrium. The dependence of the scattering and dephasing rates on electron and hole masses, plasma density, and lattice temperature is discussed.

The relaxation-time approximation is introduced and its region of validity is analyzed. Even though the RTA results show good qualitative agreement with the full results, they do not reproduce the reshaping of the kinetic hole, especially during the later stages of the relaxation process. Hence, we conclude that the RTA can be used for a simple description of the relaxation of kinetic holes in a high-density plasma, as long as the detailed shape of the kinetic hole is not significant for the processes investigated. We wish to point out, however, that our results do not imply that the RTA is valid for arbitrary initial carrier distributions. Indeed, for optical excitation of carriers high into the interband absorption region of the semiconductor, we expect quite significant deviations. This scenario will be describe in a forthcoming publication .

The results presented in this paper will be used in a variety of ongoing and future studies. As a relevant example we mention Ref. 28, where the influence of carrier dephasing on spectral hole burning and gain saturation in short-cavity semiconductor lasers is investigated.

ACKNOWLEDGMENTS

This work was supported by grants from the NSF, ARO/AFOSR (JSOP), NATO, OCC (Optical Circuitry Cooperative, University of Arizona), and through a grant for CPU time at the Pittsburgh Supercomputer Center. R.B. and K.H. acknowledge financial support by the DFG (Deutsche Forschungsgemeinschaft, Federal Republic Germany). D.S. was supported in part by the U.S. Department of Education through the Physics

Department of the University of Arizona, and K.H. thanks the Volkswagenstiftung and the Forschungszentrum Jülich for support.

APPENDIX A

The numerical solution of the Boltzmann equation (2.3) follows essentially the method of Ref. 13 for isotropic systems. After summing over $\mathbf{k}_4$ and replacing $\mathbf{k}_2$ by $\mathbf{k}_2+\mathbf{k}_1$, the polar angle between $\mathbf{k}_3$ and $\mathbf{k}_2$ is integrated with the help of the energy-conserving δ-function. The two azimuth angles are integrated trivially and only the polar angle between $\mathbf{k}_1$ and $\mathbf{k}_2$ (the cosine of which we denote by z) remains to be integrated numerically in addition to the moduli of $\mathbf{k}_2$ and $\mathbf{k}_3$. In excitonic units (i.e., the momentum is given in units of the inverse Bohr radius, energies are given in E_r, and masses are given in units of the excitonic reduced mass m_r), we have

$$\hbar\frac{df_e(k_1)}{dt}=\frac{E_r}{(2\pi)^3}\sum_\alpha\frac{m_\alpha}{2}\int_{-1}^{1}dz\int_0^\infty dk_2\,k_2\int_0^\infty dk_3(k_3+B)2|W(k_2,2k_2k_1z/m_e+k_2^2/m_e)|^2$$
$$\times\{[1-f_e(k_1)]f_e[\sqrt{k_2^2+k_1^2+2k_1k_2z}\,]$$
$$\times[1-f_\alpha(k_3+B)]f_\alpha[\sqrt{k_2^2+(k_3+B)^2-m_bA}\,]-(f\leftrightarrow 1-f)\}\ , \tag{A1}$$

with

$$A=\varepsilon_e(k_2)+\varepsilon_\alpha(k_2)+\frac{2k_1k_2z}{m_e}$$

and

$$B=m_\alpha|A|/2k_2\ .$$

The k and z integrals are performed by Gaussian quadrature. The time integration is done using a fourth-order Runge-Kutta method with an adaptive step size. The conservation of carrier density and kinetic-energy density is monitored. For the results shown, both quantities vary less than 2%. We have verified that the Fermi functions are stable even if the time integration is continued. Since with a finite number of k points the numerically obtained time derivatives never reach an exact zero, the stability of the Fermi function can in principle break down if too few k and z points are taken. Equation (A1) shows that for a finite k range the numerically more stable solution with time derivative zero is $f=$const. Upon carrier conservation this solution is only possible with a finite integration volume. In the case of the exact Boltzmann equation this solution corresponds to $f\to 0$.

The angle-integrated RPA polarization needed to evaluate the dynamically screened Coulomb potential W is given as

$$\mathrm{Re}P_\alpha(\mathbf{q},\omega)=\frac{m}{4\pi^2q}\int_0^\infty dk\,kf_\alpha(k)\ln\left[\frac{\sqrt{[\omega+\varepsilon_\alpha(q)-2qk/m_\alpha]^2+\delta^2}\sqrt{[\omega-\varepsilon_\alpha(q)+2qk/m_\alpha]^2+\delta^2}}{\sqrt{[\omega+\varepsilon_\alpha(q)+2qk/m_\alpha]^2+\delta^2}\sqrt{[\omega-\varepsilon_\alpha(q)-2qk/m_\alpha]^2+\delta^2}}\right] \tag{A2}$$

and

$$\mathrm{Im}P_\alpha(\mathbf{q},\omega)=\frac{m_\alpha}{4\pi q}\left[\int_{(m_\alpha/2q)|\omega+\varepsilon_\alpha(q)|}^\infty dk\,kf_\alpha(k)-\int_{(m_\alpha/2q)|\omega-\varepsilon_\alpha(q)|}^\infty dk\,kf_\alpha(k)\right]\ , \tag{A3}$$

where we took the limit $\delta\to 0$ in the imaginary part. The real part of P still contains δ as a parameter. We have verified, however, that for our choice of $\delta=0.05\omega_{\mathrm{pl}}$ the exact value of δ does not affect the result for W. In the limit $k_2\to 0$ a small nonzero δ can prevent W from reaching the z-independent static limit of $8\pi/\kappa^2$. We therefore force the potential to retain this limit by using a switch-off function

$$S(q)=\frac{q^a}{q^a+d^a}\ , \tag{A4}$$

where $d=\sqrt{b\kappa^2}$, and the numerical potential

$$|W^{\mathrm{num}}|^2=S|W|^2+(1-S)|W^0|^2 \tag{A5}$$

with $W^0=8\pi/(q^2+\kappa^2)$ being the statically screened potential. For the calculations discussed in Sec. III we have optimized the parameters to be $a=5.0$ and $b=0.04$ for the electron scattering rates and $b=0.12$ for the hole scattering rates, respectively.

APPENDIX B

The relaxation-time approximation (RTA) is the model of an exponential decay of a deviation $\delta f\equiv f-f^F$ from a quasiequilibrium distribution

$$f_\alpha^F(k)=\frac{1}{e^{\beta[\varepsilon_\alpha(k)-\mu_\alpha]}+1}\ , \tag{B1}$$

i.e., the Boltzmann equation reads

$$\left.\frac{df_e(k)}{dt}\right|_{cc} \simeq -\Gamma^e[k_0,f^F][f_e(k)-f_e^F(k)] , \tag{B2}$$

where the relaxation rate Γ should be evaluated at the value k_0 around which the relaxation will be studied.

Equation (B2) is an approximation to the linearized version of the original Boltzmann equation (2.3). The rigorously linearized Boltzmann equation of course contains also nondiagonal terms in k, which result from the functional derivative of the scattering rates with respect to δf. Nevertheless, one could then perform a matrix diagonalization and extract the dominant scattering rates. However, as we show in Sec. III, for the conditions analyzed in this paper a diagonal relaxation rate approximation seems quite appropriate.

The condition that Γ has to be k independent is a consequence of carrier conservation. If Γ were k dependent in the momentum region where $\delta f \neq 0$, the carrier conservation, which requires $0=(d/dt)\sum\delta f = \sum\Gamma(f-f^F)$ and simultaneously $\sum(f-f^F)=0$, could be violated,

For an efficient evaluation of the relaxation rates needed for the RTA, one can use the identity

$$f^F(\varepsilon-\hbar\omega)[1-f^F(\varepsilon)]=g(-\hbar\omega)[f^F(\varepsilon)-f^F(\varepsilon-\hbar\omega)] , \tag{B3}$$

where g is the Bose distribution

$$g(\hbar\omega)=\frac{1}{e^{\beta\hbar\omega}-1} . \tag{B4}$$

Using this identity, the definition of the RPA polarization (2.12) and the relation $|W|^2\,\mathrm{Im}P=\mathrm{Im}W$, one can rewrite the relaxation rates (2.8) and (2.9) in the following familiar form:

$$\Gamma^\alpha_{\mathrm{out}}[\mathbf{k}_1,f^F]=-2\sum_{\mathbf{k}_2}\mathrm{Im}\{W[\mathbf{k}_2-\mathbf{k}_1,\varepsilon_\alpha(k_2)-\varepsilon_\alpha(k_1)]\}g[\varepsilon_\alpha(k_2)-\varepsilon_\alpha(k_1)][1-f^F_\alpha(k_2)] \tag{B5}$$

and

$$\Gamma^\alpha_{\mathrm{in}}[\mathbf{k}_1,f^F]=-2\sum_{\mathbf{k}_2}\mathrm{Im}\{W[\mathbf{k}_2-\mathbf{k}_1,\varepsilon_\alpha(k_2)-\varepsilon_\alpha(k_1)]\}\{1+g[\varepsilon_\alpha(k_2)-\varepsilon_\alpha(k_1)]\}f^F_\alpha(k_2) . \tag{B6}$$

For practical applications of the RTA, Eq. (B2), one needs in addition to Γ^e and Γ^h also the chemical potential μ_α of the carriers and the carrier temperature $k_BT=1/\beta$, which uniquely determine the Fermi functions f_e^F and f_h^F. To obtain these parameters, we use the fact that cc scattering conserves the particle densities of electrons and holes,

$$n_\alpha=2\sum_{\mathbf{k}} f_\alpha(k) , \tag{B7}$$

as well as the total kinetic energy

$$\langle\varepsilon\rangle=\sum_\alpha\langle\varepsilon_\alpha\rangle=2\sum_{\alpha,k}\varepsilon_\alpha(k)f_\alpha(k) . \tag{B8}$$

These conditions determine μ_α and β and ensure that the carrier distributions relax toward the correct Fermi functions. If additional effects, such as the pump injection or spontaneous emission in a laser, are relevant, the outlined procedure still optimizes the RTA, even if the actual distribution function never totally agrees with the Fermi functions. Although one could just put Fermi functions into Eqs. (B7) and (B8) and solve for μ^α and T, we would like to present a numerically more practical way.

First we invert Eq. (B7) to $\beta\mu_\alpha$ for arbitrary β. To do that, we use the analytical approximation for the chemical potential discussed in Ref. 25, Chap. 6, where references to the original work are also given. According to Eq. (6.37) in Ref. 25, Eq. (B7) can be approximated by

$$\beta\mu_\alpha\simeq\ln\nu_\alpha+K_1\ln(K_2\nu_\alpha+1)+K_3\nu_\alpha , \tag{B9}$$

where $K_1=4.896\,685\,1$, $K_2=0.44\,964\,57$, and $K_3=0.133\,376\,0$. The parameter ν_α is defined by

$$\nu_\alpha=4n_\alpha\left[\frac{\hbar^2\pi\beta}{2m_\alpha}\right]^{3/2} . \tag{B10}$$

This approximation can be used in the regime $-\infty<\beta\mu_\alpha<30$. In the regime where $\beta\mu_\alpha>30$, the solution can be matched with the well-known Sommerfeld solution for low temperatures, given by

$$\beta\mu_\alpha\simeq\left[\frac{3\nu_\alpha\sqrt{\pi}}{4}\right]^{2/3}-\frac{\pi^2}{12}\left[\frac{3\nu_\alpha\sqrt{\pi}}{4}\right]^{-2/3} . \tag{B11}$$

Equations (B9) and (B11) cover the whole range excellently for Eq. (B7).

To treat Eq. (B8) the same way, we use the identity

$$\left.\frac{\partial\beta^{5/2}\varepsilon_{\mathrm{kin}}}{\partial\beta}\right|_{n_e,n_h}=\tfrac{3}{2}\beta^{3/2}\sum_\alpha\left.\frac{\partial\beta\mu_\alpha}{\partial\beta}\right|_{n_e,n_h} . \tag{B12}$$

Inserting now Eq. (B9) or Eq. (B11) into Eq. (B12) and integrating with suitable boundary conditions we obtain

$$\beta\varepsilon_{\mathrm{kin}}\simeq\tfrac{3}{2}\sum_\alpha n_\alpha\left[1+K_1-\frac{K_1}{K_2\nu_\alpha}\ln(1+K_2\nu_\alpha)+\tfrac{1}{2}K_3\nu_\alpha\right] \tag{B13}$$

for high temperatures and

$$\beta\varepsilon_{\mathrm{kin}}\simeq\sum_\alpha n_\alpha\left[\frac{3}{5}\frac{3\nu_\alpha\sqrt{\pi}}{4}\right]^{2/3}-\frac{3\pi^2}{12}\left[\frac{3\nu_\alpha\sqrt{\pi}}{4}\right]^{-2/3} \tag{B14}$$

for low temperatures, respectively. Our analysis shows that Eqs. (B12) and (B13) are excellent approximations for Eq. (B8) over the whole parameter range. These equations form a single nonlinear equation for the variable β for given n_α and $\varepsilon_{\rm kin}$, which is easy to solve numerically because the right-hand side is a monotone, smooth function. Once β is know, Eq. (B9) or Eq. (B11) is used to obtain the chemical potentials.

---

*Permanent address: Universitaet Rostock, Aussenstelle Guestrow, Physik Institut, Guestrow, Germany.

[1]For a review on photoexcited hot carriers see, e.g., J. Shah, Solid-State Electron. **32**, 1051 (1989).

[2]W. H. Knox, D. S. Chemla, G. Livescu, J. E. Cunningham, and J. E. Henry, Phys. Rev. Lett. **61**, 1290 (1988).

[3]J. L. Oudar, A. Migus, D. Hulin, G. Grillon, J. Etchpare, and A. Antonetti, Phys. Rev. Lett. **53**, 384 (1984); J. L. Oudar, A. Migus, A. Antonetti, and A. Alexandre, Phys. Rev. Lett. **55**, 2074 (1985).

[4]C. V. Shank, R. C. Fork, R. Yen, J. Shah, B. I. Greene, A. C. Gossard, and C. Weisbuch, Solid State Commun. **47**, 981 (1983).

[5]M. P. Kessler and E. Ippen, Appl. Phys. Lett. **51**, 1765 (1987).

[6]G. Böhne, T. Sure, R. G. Ulbrich, and W. Schäfer, Phys. Rev. B **41**, 7549 (1990).

[7]R. G. Ulbrich, Phys. Rev. B **8**, 5719 (1973).

[8]J. A. Kash, Phys. Rev. B **40**, 3455 (1989).

[9]W. H. Knox, C. Hirlimann, D. A. B. Miller, J. Shah, D. S. Chemla, and C. V. Shank, Phys. Rev. Lett. **56**, 1191 (1986).

[10]G. D. Mahan, *Many-Particle Physics* (Plenum, New York, 1986).

[11]L. P. Kadanoff and G. Baym, *Quantum Statistical Mechanics,* (Addison-Wesley, Reading, 1989).

[12]H. Haug and D. B. Tran Thoai, Phys. Status Solidi B **98**, 581 (1980).

[13]J. Collet and T. Amand, Physica **134B**, 394 (1985).

[14]C. Jacobini and L. Reggiani, Rev. Mod. Phys. **55**, 645 (1983).

[15]W. Schäfer, in *Festkörperprobleme (Advances in Solid State Physics),* edited by U. Rössler (Vieweg, Braunchweig, 1988), Vol. 28, p. 63; R. Binder, Ph.D. thesis, Universität Dortmund, 1988 (in German).

[16]S. M. Goodnick and P. Lugly, Phys. Rev. B **37**, 2578 (1988).

[17]M. A. Osman and D. K. Ferry, Phys. Rev. B **36**, 6018 (1987).

[18]H. Sato and Y. Hori, Phys. Rev. B **36**, 6033 (1987).

[19]T. Elsaesser, J. Shah, L. Rota, and P. Lugly, Phys. Rev. Lett. **66** 1757 (1991).

[20]C. J. Stanton, D. W. Baily, and K. Hess, Phys. Rev. Lett. **65**, 231 (1990).

[21]S. K. Lyo, Phys. Rev. B **43** 7091 (1991).

[22]S. Schmitt-Rink and D. S. Chemla, Phys. Rev. Lett. **57**, 2752 (1986); S. Schmitt-Rink, D. S. Chemla, and H. Haug, Phys. Rev. B **37**, 941 (1988).

[23]M. Lindberg and S. W. Koch, Phys. Rev. B **38**, 3342 (1988).

[24]W. Schäfer, K. H. Schuldt, and R. Binder, Phys. Status Solidi B **150**, 407 (1988).

[25]H. Haug and S. W. Koch, *Quantum Theory of the Optical and Electronic Properties of Semiconductors* (World Scientific, Singapore, 1990).

[26]R. Zimmermann and M. Hartmann, Phys. Status Solidi B **150**, 365 (1988).

[27]K. Henneberger and H. Haug, Phys. Rev. B **38**, 9759 (1988).

[28]K. Henneberger, F. Herzel, S. W. Koch, R. Binder, A. E. Paul, and D. Scott (unpublished).

[29]In Ref. (11) these scattering rates are called $\Sigma^<$ and $\Sigma^>$ and are given in Eqs. (12–19a) and (12–19b) on p. 160. The screened Coulomb potential entering the scattering rates is given as Eq. (12–20) on p. 160. In general, the spectral functions of the one-particle states entering the scattering rates are not sharp δ functions at the one-particle energies, but broadened peaks, where the broadening is itself determined by the scattering rates to be calculated [see Eq. (4.22) on p. 36 and Eq. (4.26) on p. 39 in Ref. 11]. This poses a formidable self-consistency requirement and hence even today overtaxes at least our numerical capabilities. We therefore proceed in the spirit of perturbation theory and take sharp spectral functions as the input to the scattering rates calculation.

[30]Although we have referred to Ref. 11 for the derivation of the Boltzmann equation including the screened Coulomb potential, we would like to point out that a derivation on the basis of the Keldysh Green's-function method shows in a much simpler way how the approximations for the screening function (in our case the RPA) for the scattering rates (here the Born approximation) and the one for the renormalization of the one-particle energies (which implicitly here is the screened–Hartree-Fock approximation) are actually the same approximations: the neglect of vertex corrections within the Keldysh diagram technique. In the notation of Ref. 31, this is equivalent to the approximate vertex function $\Gamma(123)$ by $-\delta(1-2)\delta(2-3)$ [see Eq. (1.15) of Ref. 31]. It follows that from a diagrammatic point of view the consistent way to treat the screening of the Coulomb potential when calculating the scattering rates within the Born approximation is to use the RPA intraband polarization function.

[31]W. Schäfer and J. Treusch, Z. Phys. B **63**, 407 (1986).